Earthquake Geotechnical Engineering for Protection and Development of Environment and Constructions – Silvestri & Moraci (Eds)
© 2019 Associazione Geotecnica Italiana, Rome, Italy, ISBN 978-0-367-14328-2

Key aspects in the engineering assessment of soil liquefaction

M. Cubrinovski, N. Ntritsos, R. Dhakal & A. Rhodes
University of Canterbury, Christchurch, New Zealand

ABSTRACT: Three important aspects in the engineering assessment of soil liquefaction, i.e. material characterization of liquefiable soils, in-situ state characterization of soils, and system response of liquefiable deposits are the subject of this paper. These aspects in the assessment are especially important in the evaluation of liquefiable soils other than uniform clean sands, such as silts, silty sands with non-plastic or low-plasticity fines, gravel-sand-silt mixtures, and interbedded deposits composed of liquefiable and non-liquefiable soils. Background of simplified liquefaction assessment procedures is first provided, and then well-documented case histories are used to demonstrate liquefaction response characteristics of actual soil deposits, and challenges encountered in their engineering evaluation. Liquefaction evaluation of gravel-sand-silt mixtures, and system response effects in liquefiable deposits are discussed somewhat in detail.

1 INTRODUCTION

In the two most recent damaging earthquakes in New Zealand, soil liquefaction was a major cause of damage to land and infrastructure. In the 2010-2011 Canterbury earthquakes, widespread liquefaction occurred in residential areas of Christchurch (Cubrinovski et al. 2011) affecting 60,000 residential buildings and properties (van Ballegooy et al. 2014), multi-storey buildings in the central area of the city (Bray et al. 2014), many bridges along the Avon River (Cubrinovski et al. 2014a), and lifeline networks throughout eastern Christchurch (Cubrinovski et al. 2014b). The economic loss due to liquefaction is estimated to be as high as 15 billion NZD or nearly 40% of the total economic loss caused by the earthquakes. In addition to the physical damage, liquefaction caused considerable long-term impacts on communities, as approximately 8,000 residential properties were abandoned in areas deemed uneconomical to recover.

In the more recent 2016 Kaikoura earthquake, liquefaction caused extensive damage in reclaimed land at the port of Wellington (CentrePort), a vital facility for the regional and national economy. Gravelly reclamations and hydraulic fills of sandy soils liquefied during the earthquake shaking causing substantial damage to wharves and buildings at the port. These recent New Zealand earthquakes clearly demonstrated that liquefaction-induced damage far exceeds tolerable levels of impacts for a modern society in spite of the significant advances in engineering assessment of liquefaction over the past 50 years.

In current engineering practice, liquefaction evaluation is commonly performed using simplified liquefaction assessment procedures, with key objectives in the assessment being to assess occurrence and effects of liquefaction, quantify damage to land and structures, and subsequently mitigate intolerable effects. To achieve these goals, reasonably accurate estimates of transient and permanent ground displacements are needed for complex ground and soil-structure systems. The important focus on displacements and damage estimates has been emphasized over the past couple of decades. Furthermore, the performance-based design framework provides means to consider the seismic performance of a given site and structure for various earthquake scenarios, and allows liquefaction effects to be considered not only in terms of physical damage, but also in terms of economic losses and impacts on communities. In spite

of this important focus on the performance evaluation through estimation of deformation, displacements and damage, one could argue that it would be difficult to achieve the required level of accuracy and meet the above objectives in the assessment without adequate consideration of essential issues in the engineering evaluation. In this paper we highlight three such issues in the assessment, namely:

1. Material characterization of liquefiable soils
2. In-situ state characterization of liquefiable soils, and
3. Consideration of cross-layer interactions and system response effects in liquefying deposits.

These issues are especially important in the evaluation of liquefiable soils other than uniform clean sands, such as silts, silty sands with non-plastic or low-plasticity fines, gravel-sand-silt mixtures, and interbedded deposits composed of liquefiable and non-liquefiable soils. In the first part of the paper, a brief overview of relevant background of simplified procedures is given, and then case histories from recent New Zealand earthquakes are used to demonstrate liquefaction response characteristics of actual soil deposits, and challenges encountered in their engineering evaluation. Even though simplified procedures are used as a basis for the discussion, the highlighted issues are equally relevant for advanced methods of liquefaction assessment.

2 SIMPLIFIED LIQUEFACTION EVALUATION PROCEDURES

The semi-empirical liquefaction evaluation procedures largely evolved around three assumptions and simplifications in the assessment:

1. Clean sand is used as a reference material in the assessment
2. Relative density is used as a principal parameter describing in-situ state of the soil, and
3. Each layer is evaluated independently, and in isolation, without consideration of the response and effects of other layers within the profile or the deposit as a whole.

These simplifications are directly related to the identified three aspects in the assessment (i.e. material characterization, in-situ state characterization and system response of liquefiable deposits), and are discussed in the following subsections. Note that other important assumptions and considerations in the simplified procedures are beyond the scope of this paper.

In what follows, CPT-based triggering procedures are used as a basis for the discussion, though the presented arguments are equally valid for alternative SPT- and V_s-based liquefaction triggering methods. Figure 1a shows CPT-based liquefaction triggering correlation proposed by Boulanger & Idriss (2014) expressed in terms of corrected *equivalent clean sand* cone tip resistance q_{c1Ncs}, for earthquake magnitude $M_w = 7.5$ and effective overburden stress $\sigma'_v = 100$ kPa. The correlation shown with the solid line can be used to estimate the liquefaction resistance $CRR = CSR_{Mw=7.5,\ \sigma'v\ =\ 100}$, if q_{c1Ncs} for any given layer (depth) is estimated from CPT data.

2.1 *Clean sand as a reference material*

In the triggering correlation of Boulanger & Idriss (2014), q_{c1Ncs} is calculated by correcting the measured penetration resistance for the effects of fines content using the following expression:

$$q_{c1NcS} = q_{c1N} + \Delta q_{c1N} \tag{1}$$

Here, q_{c1N} is normalized penetration resistance obtained directly from measured cone tip resistance (q_c), and Δq_{c1N} is correction for the effects of fines content (FC). For clean sand, there is no correction, so $q_{c1Ncs} = q_{c1N}$. However, for fines-containing sand Δq_{c1N} increases with fines content, and the correction is significant. For example, as illustrated in Figure 1b, for sand with $FC = 35\%$ and $q_{c1N} = 92$, the adjusted q_{c1Ncs} is 1.65 times greater than the

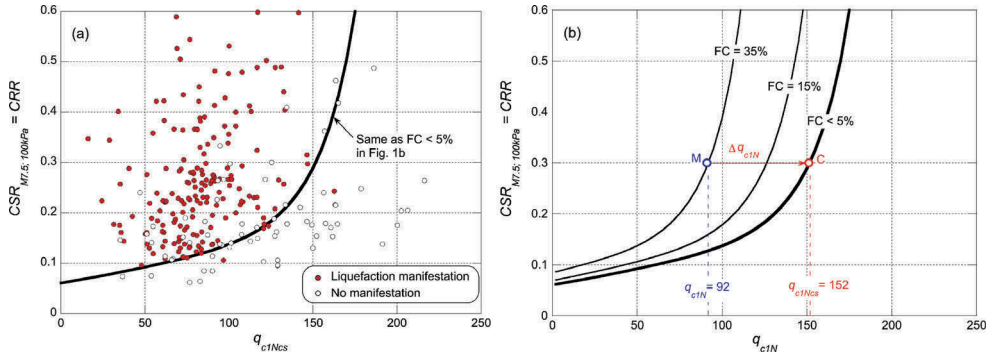

Figure 1. CPT-based liquefaction triggering correlation of Boulanger and Idriss (2014), for M_w = 7.5 and σ'_v = 100 kPa: (a) expressed in terms of corrected equivalent clean sand cone tip resistance q_{c1Ncs}; (b) expressed in terms of q_{c1N} for FC < 5% (clean sand), FC = 15% and FC = 35%; a correction of penetration resistance Δq_{c1N} for FC = 35% is illustrated with the shift from point M (measured q_{c1N} = 92) to point C (corrected q_{c1Ncs} = 152).

'measured' q_{c1N} value. Such corrections for the effects of fines content can exceed a factor of 3 for low q_{c1N} values. In essence, there is a significant adjustment of the liquefaction triggering correlation based solely on the fines content, which has been adopted as a sole measure for material characteristics differentiating from clean sand.

The original correlations established from liquefaction case histories by Boulanger & Idriss (2014) are shown in Figure 1b in terms of normalized cone tip resistance q_{c1N}, for clean sand (FC < 5%), FC = 15% and FC = 35%. An increase in the fines content shifts the correlation upward and to the left from the reference clean sand relationship (FC < 5%). This shift in the correlation could be due to effects of fines on the liquefaction resistance (i.e. $CRR = f(FC)$), effects of fines on the penetration resistance (i.e. $q_{c1N} = f(FC)$), or due to combined effects of FC on q_{c1N} and CRR. It will be shown in Section 3.4 of this paper that the shift in the correlation seen in Figure 1b does not reflect the effects of fines on liquefaction resistance, but rather is predominantly due to grain-size effects on penetration resistance of soils.

2.2 *Relative density as a principal state parameter*

One of the key reasons for the use of clean sand as a reference material in the liquefaction assessment was that the majority of liquefaction case histories in the initial database were on clean sands and sands with small amounts of fines. Hence, the focus on clean sands was driven by the early evidence that sands have high liquefaction potential. One important corollary is that relative density (D_r) has been implicitly adopted as a reference state parameter in liquefaction assessment. Relative density is established as a parameter that works well for sands, as it represents the density state of sand, which in turn strongly influences sand behaviour under monotonic and cyclic shearing. Consequently, there is a strong correlation between liquefaction resistance (CRR) and relative density (D_r) of sand, as illustrated in Figure 2a. Here, conventional empirical relationships between relative density and cone tip resistance for clean sand, given in Equations 2 and 3 (Idriss & Boulanger 2008; Tatsuoka et al. 1990; Zhang et al. 2004), were used to convert q_{c1Ncs} into D_r, and then replot the CRR - q_{c1Ncs} liquefaction triggering correlation of Boulanger and Idriss (2014) in Figure 2a, in terms of CRR - D_r.

$$D_r = \left\{0.478(q_{C1Ncs})^{0.264} - 1.063\right\} \cdot 100 \tag{2}$$

$$D_r = -85 + 76\log(q_{C1Ncs}) \tag{3}$$

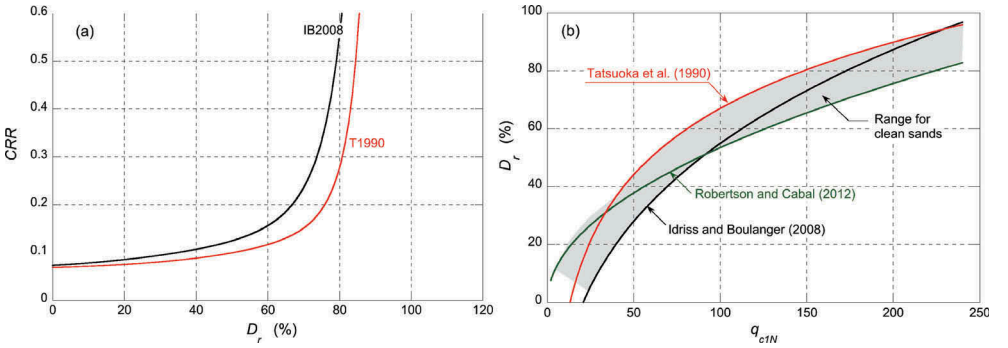

Figure 2. Relative density as a measure for in-situ state of the soil in liquefaction assessment: (a) Boulanger and Idriss (2014) liquefaction triggering correlation expressed in terms of relative density (D_r) using empirical expressions provided by Idriss & Boulanger (2008) and Tatsuoka et al. (1990); (b) relationships between D_r and q_{c1N} for clean sand used in liquefaction evaluation.

The D_r - q_{c1N} relationships of Equations 2 and 3 are depicted in Figure 2b together with the relationship proposed by Robertson & Cabal (2012). The pronounced sensitivity of the penetration resistance to changes in relative density shown in Figure 2b has been one of the principal reasons for its use in the liquefaction assessment as a proxy for the in-situ density of the soil. Thus, we rely on the penetration resistance to differentiate between loose and dense soils or low and high liquefaction resistance respectively. However, at present, it is difficult to apply the relative density concept to soils other than clean sands, as standard procedures for evaluation of index void ratios (e_{max} and e_{min}), required in the calculation of D_r, are not available for such soils. Furthermore, there is a convincing evidence that the state concept interpretation of soil behaviour provides a more robust framework for characterization of the in-situ state of soils, as it neatly combines effects of density and confining stress on the stress-strain behaviour of soils.

The above discussion implies that, generally, material and state characterization for fines-containing soils or any liquefiable soil distinctly different from clean sand is not of the same quality and accuracy as that of clean sand.

2.3 *Evaluation of liquefaction response without consideration of cross-layer interactions*

The third important feature in simplified liquefaction evaluation is schematically illustrated in Figure 3 for a six-layer soil profile, in which layers 3 and 5 are liquefiable, whereas layers 1, 2, 4 and 6 are non-liquefiable. In the simplified procedure each layer is considered in isolation, and a factor of safety against liquefaction triggering (*FS*), and consequent maximum shear (γ_{max}) and volumetric strains (ε_v) are estimated separately for each layer. Thus, when calculating *FS*, γ_{max} and ε_v for any given layer, the response and effects of other layers or interactions between layers within the deposit are ignored. In the subsequent step, liquefaction damage indices, such as LSN (van Ballegooy et al. 2014) and LPI (Iwasaki et al. 1978; Maurer et al. 2014) are calculated using specific weighting functions to quantify the damage potential of liquefying layers depending on their proximity to the ground surface. But still, when calculating the damage indices, a simple superposition of previously calculated independent effects is used, as illustrated in Figure 3b, and cross-interactions between layers through the dynamic response and liquefaction effects are simply ignored.

We can summarize the key elements of the three simplifications in the assessment, as follows:

1. Clean sand is essentially used as a reference material, and fines content is used as a sole measure for material characteristics differentiating from clean sand; the liquefaction resistance is very sensitive to fines content in empirical *CRR* - q_{c1N} relationships.

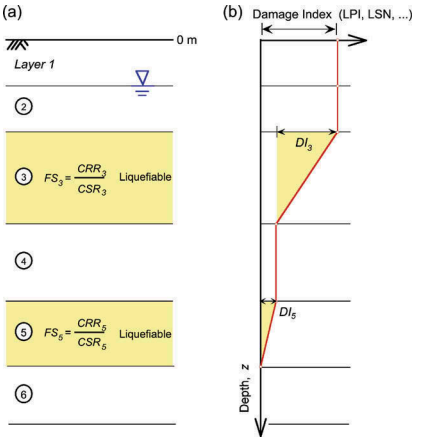

Figure 3. Schematic illustration of liquefaction assessment using simplified approach: (a) factors of safety against liquefaction triggering are calculated independently for each layer; (b) cumulative damage index is calculated for the deposit (site) by superposition of individual effects from each layer.

2. Relative density is implicitly used as the principal measure for the in-situ state of the soil through penetration resistance; relative density is a well-established concept for clean sands, but its application to any soil other than clean sand is not straightforward.
3. Finally, cross-layer interactions and overall response of the deposit are not considered in the evaluation of the liquefaction response.

In the following sections, we will further explore these issues using well-documented liquefaction case histories from recent New Zealand earthquakes.

3 MATERIAL AND STATE CHARACTERIZATION OF GRAVEL-SAND-SILT MIXTURES

3.1 *Liquefaction of reclaimed land*

In the 2016 M_w7.8 Kaikoura earthquake, widespread liquefaction occurred in reclamations of Wellington port (CentrePort). The liquefaction was particularly extensive and severe in the gravelly fills of Thorndon reclamation (Cubrinovski et al. 2017; 2018a). This reclamation was constructed between 1965 and 1976 by end-tipping approximately 2,900,000 m^3 of gravelly soils sourced from nearby quarries. Soft marine sediments were first removed from the seabed by dredging, and then the quarry material was dumped into the sea from truck and barge operations, thus constructing a 10 m to 20 m thick fill through a water sedimentation process. Static rollers were used to compact the top 2-3 m of the fill as soon as the fill surfaced above high-tide water level. Hence, the fill below 2-3 m depth is uncompacted. The reclamation is laterally unconfined in three directions (east, south and west) with relatively steep original slopes (1.5H:1V). The fill overlies 1-5 m thick marine sediments of interbedded sand, clay and silty clay that sit on top of the Wellington Alluvium formation, which comprises stratified dense gravels and stiff to very stiff silts.

Despite the relatively moderate peak ground accelerations of about 0.20 g at the ground surface (Bradley et al. 2017), extensive liquefaction occurred in the gravelly reclamation during the Kaikoura earthquake. The liquefaction manifestation varied from traces of ejected silts and water, to large volumes of soil ejecta with thicknesses of up to 150-200 mm. Figure 4 shows images of gravelly ejecta observed at the Thorndon Terminal which are illustrative of the worst affected areas. Large volumes of gravelly ejecta were found along cracks and fissures in the pavement, cavities and along drainage lines, which created preferred pathways for

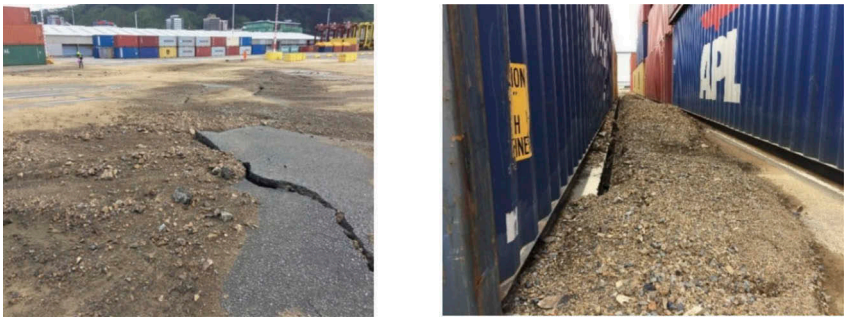

Figure 4. Liquefaction manifestation at CentrePort observed after the 2016 Kaikoura earthquake.

groundwater flow and soil ejecta to reach the ground surface. Visually, the ejecta appeared as a well-graded gravelly soil including some cobble-size particles, but also sand and silt.

The liquefaction resulted in large permanent ground displacements and global deformation pattern of the gravelly reclamation, as schematically depicted in Figure 5. It involved an outward (seaward) movement of the reclamation slopes (edges), with lateral spreading producing maximum ground displacements near the edges of the fill (slope crest), and consequent cracking and ground distress progressing in-land within the reclamation. The outward displacement of the fill was accompanied by a slumping mode of deformation involving global (mass) settlement of the reclamation. As shown in Figure 5, the settlement in the central part of the reclamation was on the order of 0.2-0.3 m, whereas it increased near the reclamation edges to 0.4-0.6 m due to spreading-induced movements. The large ground displacements caused substantial damage to paved surfaces and buildings on shallow and deep foundations at the port, and damaged beyond repair two pile-supported wharves, which displaced 0.5-1.5 m laterally towards the sea. Detailed account of the observed damage to land and structures at CentrePort can be found in Cubrinovski et al. (2017).

3.2 *Material characteristics of gravel-sand-silt mixtures*

There are many interesting aspects of the liquefaction at CentrePort, but we will focus our attention on the identified issues around material and state characterisation in the liquefaction assessment. After the earthquake, gravelly ejecta samples were collected from 15 locations at the port for sieve analyses. Grain size distribution (GSD) curves of the collected samples are shown with solid lines in Figure 6, whereas the shaded area in the background depicts the range of GSD curves of borehole samples, which were collected several years before the earthquake. The fill is a gravel-sand-silt mixture consisting predominantly of gravels (i.e. approximately 45-75% gravel, 15-40% sand and 10-15% fines). The good agreement between the two sets of GSD curves confirms that the ejecta samples have similar grain-size composition as the original fill, and that the gravel-sand-silt mixture indeed liquefied during the earthquake.

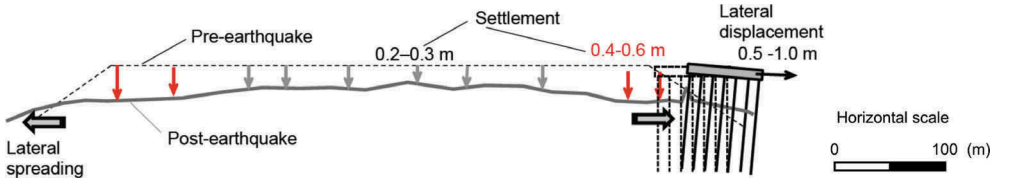

Figure 5. Global deformation pattern involving settlement (slumping) and lateral spreading of gravelly reclamation.

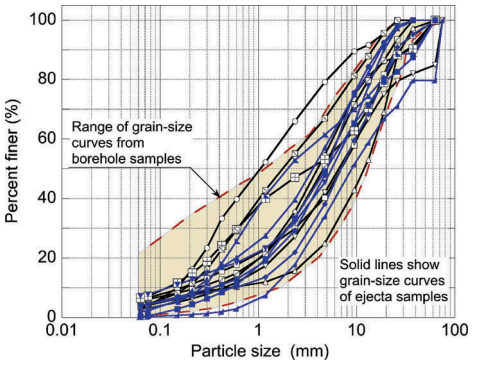

Figure 6. Grain-size distribution (GSD) curves of samples from gravelly reclamation at CentrePort; solid lines show GSD curves of ejecta samples; shaded area indicates range of GSD curves of borehole samples.

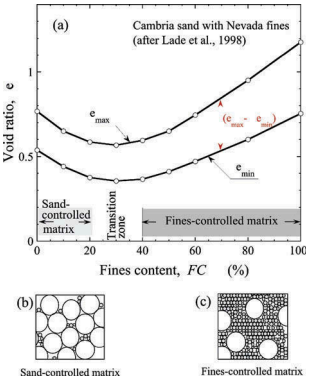

Figure 7. Influence of fines content on the packing of sand-silt mixtures: (a) variation of index void ratios with fines content for Cambria sand – Nevada silt mixtures; (b) sand-controlled matrix for $FC < 20\%$; (c) fines-controlled matrix for $FC > 40\%$ (Cubrinovski & Ishihara 2002; after Lade et al. 1998).

Liquefaction assessment of gravel-sand-silt mixtures using simplified procedures is not straightforward, as such soils effectively are not represented in the empirical database. However, there is one important characteristic in the grain-size composition of the fill that one could make use of. Namely, even though the fill is dominated by gravels, there is a sufficiently large amount of sand and non-plastic silt for these finer fractions to influence the behaviour of the fill during earthquakes. This interpretation is based on findings from several comprehensive laboratory studies in which sand-silt mixtures were investigated by mixing a specific amount of silt with host sand. Figure 7a shows one result from such a study where index void ratios (e_{max} and e_{min}) are plotted against the fines content, for a sand-silt mixture. The plot essentially illustrates effects of fines content on the packing of sand-silt mixtures. Conceptually, when the fines content is relatively small ($FC < 20\%$), the microstructure (and hence deformational behaviour) of the mixture is controlled by the sand matrix, as illustrated schematically in Figure 7b for an idealized binary packing of spherical particles. Conversely, at fines content $FC > 40\%$, the microstructure is effectively controlled by the silt matrix, in which case the coarse grains (sand particles) are separated by finer grains (silt particles), as depicted in Figure 7c. As indicated in Figure 7a, there is a transition in the microstructure from sand-controlled matrix to fines-controlled matrix as the fines content increases from approximately 20% to 40%. Analogous to this interpretation for sand-silt mixtures, the 30% or more amount of sands and silts in the gravelly fill at CentrePort are considered sufficient for these finer fractions to control the soil matrix and have a critical influence on the liquefaction resistance and behaviour of the gravelly fill during earthquakes. With this background in mind, comprehensive CPT investigations were performed to characterize the gravelly reclamations at CentrePort (Cubrinovski et al. 2018a; Dhakal et al. 2019).

3.3 *In-situ state characterization of gravelly fill*

About 60 CPTs were performed at CentrePort in the gravelly reclamation. Tests were performed with 10 cm^2 and 15 cm^2 cones, and field operations involved predrilling to a depth of approximately 3 m through asphalt pavement and dense compacted gravelly crust using a plugged casing with an extractable tip (Cubrinovski et al. 2018a). If early refusal was encountered during a test at depths less than approximately 10 m, the casing was pushed through the high-resistance soils beyond the depth of refusal, and then cone testing was resumed. A

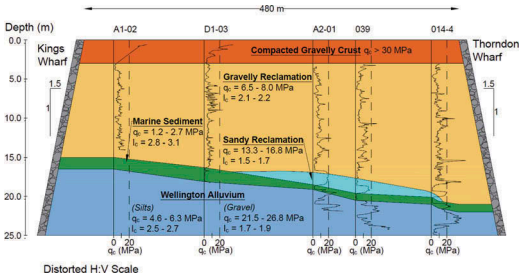

Figure 8. East-west cross-section through the gravelly fill of Thorndon reclamation showing CPT q_c traces and summary of representative q_c and I_c values (25th and 75th percentile values) for characteristic soil units (Dhakal et al. 2019).

characteristic cross section through the gravelly reclamation derived from the CPT data is shown in Figure 8.

Careful examination of q_c traces reveals that the gravelly fill predominantly exhibited low cone tip resistance of q_c = 6.5-8.0 MPa, which represent the 25th and 75th percentile q_c values, respectively. The low penetration resistance implies low density of the fill, which is consistent with the employed construction method, sedimentation of soil particles through water, and their deposition in a relatively loose state, without any external compaction effort.

The CPT data yielded soil behaviour type index values of I_c = 2.1-2.2 for the gravel-sand-silt mixture, which imply soil behaviour consistent with sand-silt mixtures (Robertson & Wride, 1998). Indeed, the CPT data obtained in the gravelly fill are characteristic for a sand-silt mixture, and the influence of gravel is only occasionally apparent as spikes in the q_c trace when gravel particles are encountered by the cone tip. This CPT-based interpretation is consistent with the anticipated governing influence of sand-silt fractions in the soil matrix implied previously based on the grain-size composition of the mixture (i.e. the presence of 30% or more sands and silts in the fill), and is also in agreement with the observed performance of the reclamation during the 2016 Kaikoura earthquake, which exhibited liquefaction severity more typical for sand-silt mixtures rather than gravels. Figure 9 shows details of two additional CPT profiles in the gravelly fill to better illustrate some of the CPT characteristics discussed above.

Hence, general applicability of simplified liquefaction assessment procedures to the gravel-sand-silt reclamation could be justified based on the governing influence of the sand-silt fractions in the soil matrix. However, evaluation of the in-situ density state of the gravelly fill is

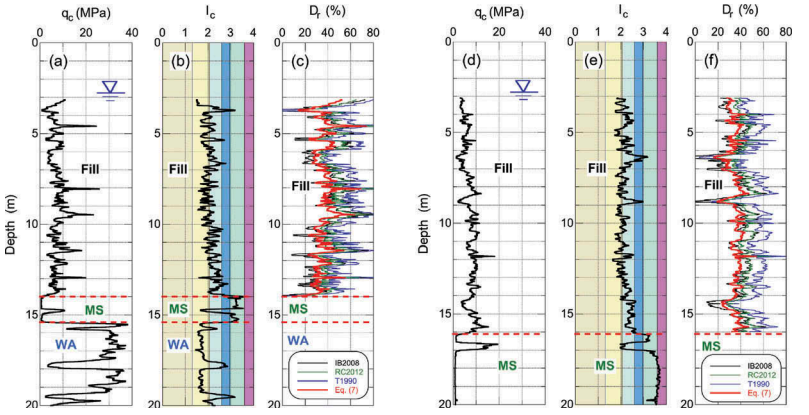

Figure 9. Measured cone tip resistance (q_c), soil behaviour type index (I_c), and estimated relative density (D_r) of the gravelly fill: (a, b, c) CPT045; (d, e, f) CPT021.

still problematic because of the difficulties in determining index void ratios for gravelly soils and evaluating the influence of grain size on the penetration resistance of soils (e.g. Skempton 1986; Tokimatsu 1988; Cubrinovski & Ishihara 1999). To estimate the density state of the fill, relative density profiles for the fill were calculated using relationships for clean sand illustrated in Figure 2b, which strictly speaking are not directly applicable for the gravel-sand-silt reclamation. The relative density of the fill was also estimated using an empirical correlation that was developed for a wide range of liquefiable soils including silty sands, clean sands and gravels (Cubrinovski & Ishihara 1999). The latter correlation was derived from a comprehensive study on the effects of grain-size characteristics of sandy soils (including clean sands, sands with fines and gravelly sands) on the packing of soils (Cubrinovski & Ishihara 2002), steady state characteristics of soils (Cubrinovski & Ishihara 2000) and penetration resistance of soils (Cubrinovski & Ishihara 1999). Cubrinovski & Ishihara (1999) proposed penetration resistance – relative density correlation using data from high-quality samples recovered by ground freezing and SPT data with energy ratio of 78%, shown in Figure 10a. The correlation has the following original form:

$$(N_1)_{78} = D_r^2 \frac{9}{(e_{max} - e_{min})^{1.7}} \tag{4}$$

which for a conventional 60% energy ratio becomes:

$$(N_1)_{60} = D_r^2 \frac{11.7}{(e_{max} - e_{min})^{1.7}} \tag{5}$$

To convert $(N_1)_{60}$ into q_{c1N}, a link between the CPT-based and SPT-based triggering correlations of Boulanger & Idriss (2014) via *CRR* could be used resulting in the $QNR = q_{c1N}/(N_1)_{60}$ ratios shown in Figure 10b. According to the Boulanger & Idriss (2014) relationships, $QNR \approx 8$ for $q_{c1Ncs} < 100$, and the ratio steadily decreases to a value of about 6 for $q_{c1Ncs} = 150$. Note however that Robertson et al. (1983) have shown that *QNR* depends on the mean grain size of soils, and that *QNR* increases with increasing grain size of soils. Robertson (2012) provided an updated relationship for *QNR* using I_c, in which *QNR* ranges from approximately 3 to 7, for fine-grained to coarse (gravels) liquefiable soils, respectively. To allow for different considerations of grain-size effects on *QNR*, the above correlation between the penetration resistance and relative density of Cubrinovski & Ishihara (1999) can be expressed in terms of cone tip resistance (q_{c1N}), using a generic $QNR = q_{c1N}/(N_1)_{60}$ term, as:

$$q_{c1N} = D_r^2 \frac{11.7 \cdot QNR}{(e_{max} - e_{min})^{1.7}} \tag{6}$$

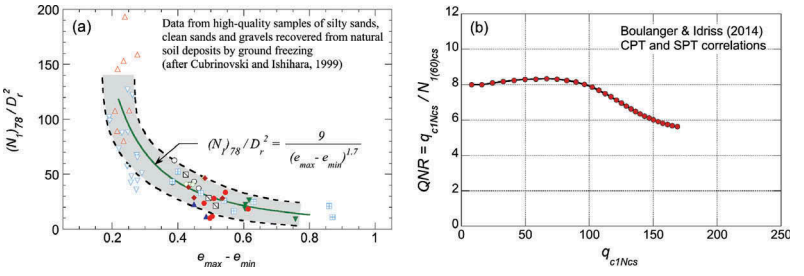

Figure 10. (a) Empirical correlation between SPT blow count and relative density of granular soils (Cubrinovski & Ishihara 1999); (b) $QNR = q_{c1Ncs}/(N_1)_{60cs}$ ratios derived from Boulanger & Idriss (2014) CPT and SPT triggering relationships.

or if solved for D_r as:

$$D_r = \left\{ \frac{1}{11.7 \cdot QNR} \cdot q_{c1N} \cdot (e_{max} - e_{min})^{1.7} \right\}^{0.5} \tag{7}$$

This relationship uses the void ratio range ($e_{max} - e_{min}$) as a measure for the material characteristics of soils instead of conventional GSD curve parameters such as FC or D_{50}, as ($e_{max} - e_{min}$) reflects the effects of overall grain-size composition and particle characteristics (shape) of soils. Relationships ($e_{max} - e_{min}$) - FC, and ($e_{max} - e_{min}$) - D_{50} have been also provided (Cubrinovski & Ishihara 1999; Cubrinovski & Ishihara 2002) to facilitate the use of the relationship in practice via FC and D_{50}, for cases where index void ratios are not available from laboratory testing.

Relative density estimates for the gravelly fill are shown in Figure 9c and 9f, based on the previously introduced clean sand relationships, and the relationship from Equation 7 for $QNR = 6$ and ($e_{max} - e_{min}$) = 0.30, which are considered representative for the gravelly fill. The latter relationship yields a low relative density of the fill of about $D_r = 40\%$, which appears consistent with the deposition of large volume of soils through water sedimentation, and lack of compaction effort in the construction of the reclamation. It is apparent that clean sand relationships generally estimate higher relative density of the fill as they ignore grain-size effects on penetration resistance.

The material and state characterization of the gravel-sand-silt mixtures discussed above, highlight the need to carefully consider soil composition and consequently which portion of the soil matrix is controlling the behaviour during earthquakes, and then evaluate the in situ state of the soil while allowing for such compositional factors and effects in the engineering interpretation.

3.4 *Empirical liquefaction triggering correlation expressed in terms of relative density*

The above empirical correlation between penetration resistance and relative density can be used to scrutinize the shift in the liquefaction triggering correlation with the fines content shown in Figure 1b. Using the expression given in Equation 7, $q_{c1N} - D_r$ relationships are plotted in Figure 11 for clean sand ($FC = 0\%$), sand with $FC = 15\%$ and $FC = 35\%$, and also gravelly sand, through the use of representative ($e_{max} - e_{min}$) values for these soils. In Figure 11a and 11b, $QNR = 6$ and $QNR = 8$ were used respectively. Note that $QNR = 6$ provides better agreement with empirical $q_{c1N} - D_r$ relationships for clean sand, whereas $QNR = 8$ is more representative of the ratios derived from the Boulanger & Idriss (2014) triggering relationships, for $q_{c1Ncs} < 100$. Regardless of the adopted value for QNR, the trend in both sets of relationships consistently shows that, at a given relative density, penetration resistance of sand decreases with increased fines content. Conversely, an increase in gravel content or increase in

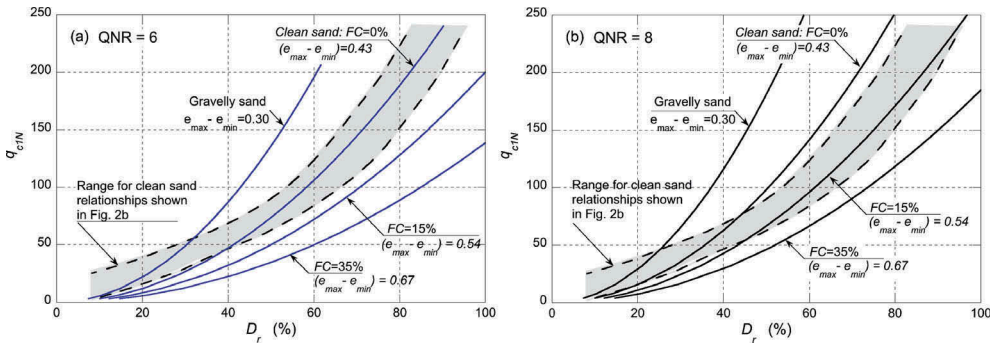

Figure 11. Relationships between penetration resistance q_{c1N} and relative density of sandy soils illustrating influence of grain size on the penetration resistance of soils (Cubrinovski & Ishihara 1999): gravelly sand with ($e_{max} - e_{min}$) = 0.30; clean sand with ($e_{max} - e_{min}$) = 0.43; sand with $FC = 15\%$ or ($e_{max} - e_{min}$) = 0.54 and $FC = 35\%$ or ($e_{max} - e_{min}$) = 0.67; (a) QNR = 6; (b) QNR = 8.

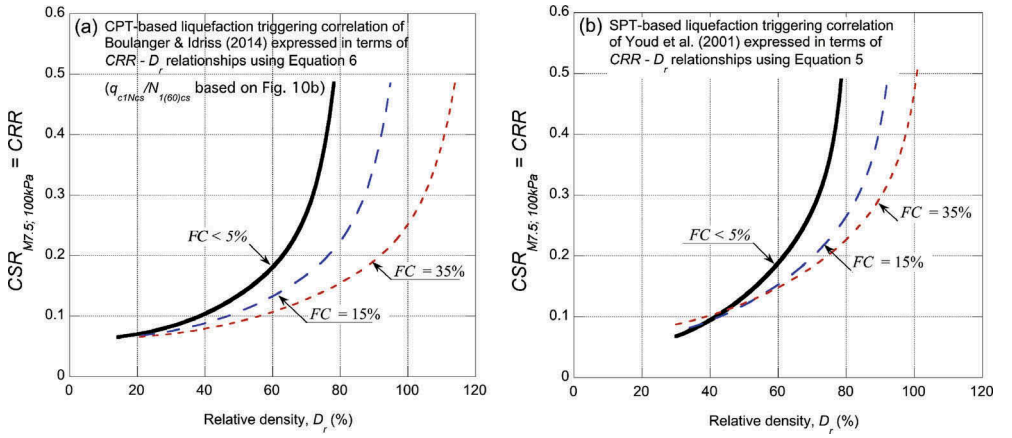

Figure 12. Empirical liquefaction triggering correlations for clean sand and sand with fines expressed in terms of relative density: (a) Boulanger & Idriss (2014) CPT-based relationships; (b) Youd et al. (2001) SPT-based relationships.

the grain-size of soil causes an increase in the penetration resistance. These effects of grain-size composition of soils on the penetration resistance are significant.

Equations 5 and 6 can be further used to directly express empirical SPT-based and CPT-based liquefaction triggering correlations in terms of the relative density. For example, using Equation 6 together with the $CRR = f(q_{c1Ncs})$ empirical expression of Boulanger & Idriss (2014), their CPT-based liquefaction triggering correlations for clean sand ($FC = 0\%$), sand with $FC = 15\%$ and $FC = 35\%$ were plotted in Figure 12a against D_r. In these plots, varying $QNR = q_{c1Ncs}/(N_1)_{60cs}$ ratios as defined in Figure 10b were used. Similarly, Figure 12b shows empirical SPT-based triggering correlations of Youd et al. (2001) expressed in terms of D_r using Equation 5. Both plots show identical trends and effects of fines content on the liquefaction resistance:

1. At low relative density, approximately $D_r < 40\%$, clean sand and sands with up to 35% fines show similar liquefaction resistance.
2. For relative densities $D_r > 50\%$, a pronounced decrease in liquefaction resistance is seen with an increased fines content.

These results are largely in agreement with evidence from laboratory studies and also are consistent with a more rigorous state concept interpretation of stress-strain behaviour of clean sands and sands with fines. They also implicitly suggest that the substantial shift in the empirical liquefaction triggering correlation with increased fines content seen in Figure 1b is indeed caused by a decrease in the penetration resistance due to increased fines content in soil.

4 SYSTEM RESPONSE OF LIQUEFIABLE DEPOSITS

4.1 *Liquefaction observations from the 2010-2011 Canterbury earthquakes*

The final aspect to be discussed herein is the importance to consider cross-layer interactions and overall response of the deposit in the evaluation of liquefaction. Evidence and findings from the Canterbury earthquakes have shown that characteristics of the soil deposit, its overall dynamic and liquefaction response features, and effects of cross-layer interactions can significantly influence and even govern the severity of liquefaction manifestation at the ground surface.

After the 2010-2011 Canterbury earthquakes, comprehensive studies were carried out to scrutinize the accuracy of simplified liquefaction evaluation procedures in predicting liquefaction triggering (manifestation) and associated damage. These studies found that although the

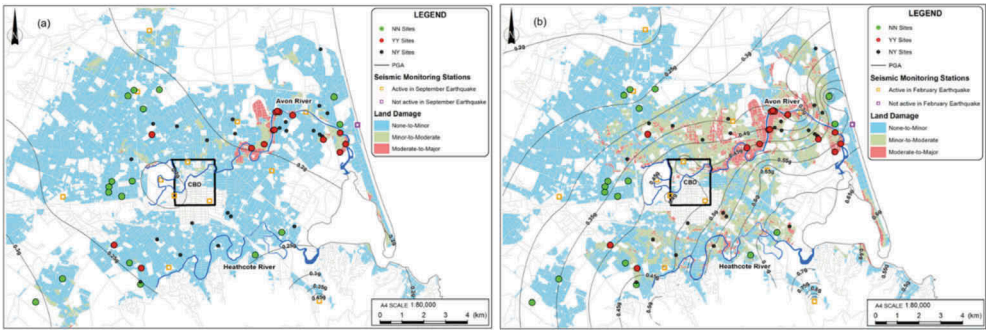

Figure 13. Land damage maps indicating none-to-minor, minor-to-moderate, and moderate-to-major liquefaction in: (a) 4SEP2010 (Darfield) earthquake; (b) 22FEB2011 (Christchurch) earthquake; PGA contours and locations of 55 investigated sites are also shown (Cubrinovski et al. 2018b).

simplified procedures could capture general trends in the observed liquefaction damage, there were a significant number of predictions that were inconsistent with field observations. Importantly, biases in the predictions were seen with systematic mispredictions of occurrence and severity of liquefaction for specific areas and certain types of deposits. For example, simplified procedures erroneously predicted that moderate to severe liquefaction damage should have occurred over large areas in the suburbs south of the CBD during the Darfield earthquake (4 September 2010 earthquake), e.g. Beyzaei et al. (2018). However, as illustrated in Figure 13a, no such damage was observed in these parts of Christchurch after this earthquake.

To investigate the reasons for systematic mispredictions by the simplified methods, a comprehensive study was performed using 55 well-documented case history sites that showed vastly different performance during the earthquakes, from no liquefaction manifestation to extreme severity of liquefaction manifestation (Cubrinovski et al. 2018b). Based on the observed liquefaction manifestation, the 55 sites were classified into three groups: (i) sites that manifested liquefaction (soil ejecta) in both 4 September 2010 and 22 February 2011 earthquakes ('Yes-Yes' or YY-cases, shown with red symbols in Figure 13); (ii) sites that did not manifest liquefaction in the 4 September 2010 event, but manifested liquefaction in the 22 February 2011 earthquake ('No-Yes' or NY-cases; black symbols); and, (iii) sites that did not manifest liquefaction in any event during the 2010-2011 Canterbury earthquakes ('No-No' or NN-cases; green symbols).

4.2 *Critical layer characteristics*

To investigate the reasons for the dramatic difference in liquefaction manifestation (damage) amongst these sites, detailed field investigations were performed at each of the 55 sites using CPT, V_s and V_p cross-hole measurements. Using the CPT data, simplified soil profiles were determined for each site, in which characteristic soil layers were identified throughout the profile, and representative thickness, cone tip resistance (q_c) and soil behaviour type index (I_c) were assigned to each layer. In the subsequent step, for each site the simplified soil profile and results from conventional triggering analyses were used to identify the critical layer within the profile or the layer that is the most likely to trigger and manifest liquefaction at the ground surface (Cubrinovski et al. 2018b).

Somewhat surprisingly, we found no significant difference between the properties of the critical layers of YY-sites (which manifested liquefaction in both earthquakes) and NN-sites (which did not manifest liquefaction in any earthquake). Indeed, the YY-sites and NN-sites have identical critical layers in terms of their median CPT values ($q_{c1Ncs} \approx 86$ and $I_c \approx 2.15$), and depth of the critical layer ($z_{CL} \approx 2.1$ m). Hence, the dramatic difference in observed liquefaction manifestation at the YY-sites and NN-sites cannot be explained through differences in

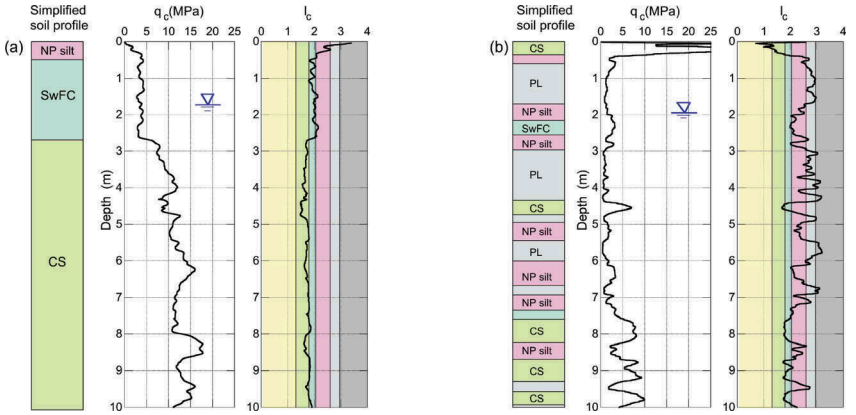

Figure 14. Characteristic CPT and soil profiles for: (a) sites that liquefied in both major earthquakes (YY); (b) sites that did not liquefy in any of the 2010-2011 earthquakes (NN); (Cubrinovski et al. 2018b).

the characteristics of their critical layers. Consequently, liquefaction manifestation predictions from simplified analyses were generally inconsistent with observations at NN-sites and YY-sites. Importantly, there was a systematic bias in the predictions by the simplified procedures. For NN-sites, liquefaction manifestation was overestimated for 91% of the cases, whereas for YY-sites, severity of liquefaction manifestation was underestimated for 37% of the cases.

4.3 *Deposit characteristics*

While YY-sites and NN-sites have identical characteristics of their critical layers, there are clear differences in their overall deposit characteristics. As shown in Figure 14a, sites that manifested liquefaction in both major earthquakes (YY-sites) are characterized by vertically continuous liquefiable soils in the top 10 m. These deposits are typically composed of a shallow silty sand in the top 2-3 m, overlying a vertically continuous 7 m to 8 m thick sand or fine sand layer.

The sites that did not manifest liquefaction in any of the 2010-2011 earthquakes (NN-sites), on the other hand, are characterized by highly stratified deposits comprising interbedded liquefiable and non-liquefiable soils, as shown in Figure 14b. A crust of non-liquefiable soil, horizontal 'grid' of non-liquefiable layers and consequent vertical discontinuity of liquefiable soils are key features of the NN-sites. At both YY- and NN-sites the water table is shallow, at about 2 m depth. However, V_p profiles indicated different degrees of saturation in the shallow part of the YY- and NN-deposits. Full saturation was implied in vertically continuous liquefiable sands at YY-sites for all soils deeper than 0.5 m below the water table, whereas the presence of non-liquefiable layers at NN-sites resulted in partial saturation for soils up to 3 m to 5 m below the water table.

To investigate more rigorously the response induced by the earthquakes for these two types of deposits, a comprehensive series of seismic effective stress analyses were performed (Cubrinovski et al. 2018b). In these response history analyses, key features of the soil response and liquefaction process such as build-up of excess pore water pressures, reduction in soil stiffness and strength, and redistribution of pore water pressures through water flow are rigorously modelled. Hence, the analyses account for interactions between layers through the dynamic response and water flow effects in liquefying deposits.

Two soil-column (1-D) models used in the analyses, representative of YY and NN deposits, are shown in Figure 15. The models have nearly identical critical layers in terms of liquefaction resistance (as represented by q_{c1Ncs}) and location of the critical layer within the deposit. However, they have different deposit characteristics, i.e. vertically continuous liquefiable sands for the YY-deposit, and stratified deposit with liquefiable and non-liquefiable layers,

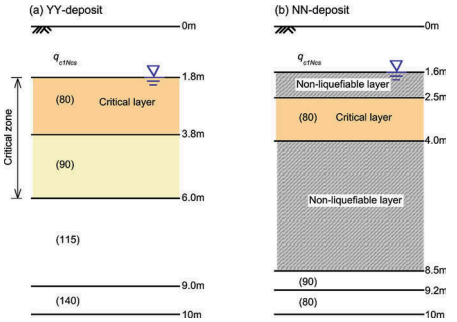

Figure 15. Soil-column models used in the seismic effective stress analyses representative of: (a) vertically continuous liquefiable soils of YY-deposits; (b) stratified liquefiable and non-liquefiable soils of NN-deposits (Cubrinovski et al. 2018b).

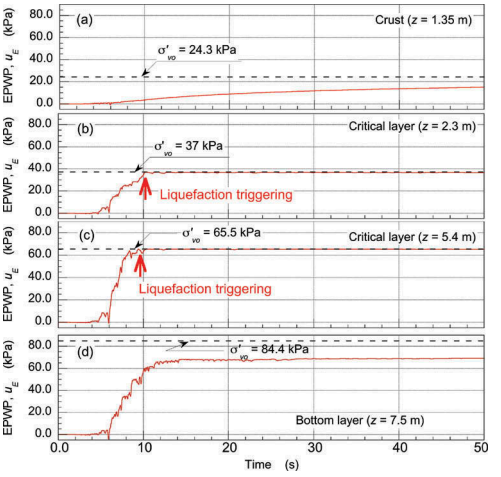

Figure 16. Excess pore water pressure time histories computed throughout the depth of YY-deposit that liquefied during the Canterbury earthquakes: (a) crust above water table; (b), (c) critical layer (zone); (d) deeper sand layers beneath the critical zone.

for the NN-deposit. Details on the seismic effective stress analyses can be found in Cubrinovski et al. (2018b), whereas herein only key results and findings from these analyses are presented.

4.4 *System response effects intensifying liquefaction manifestation*

In the following, we will briefly examine only key elements in the seismic response and evolution of liquefaction effects obtained in the analyses of the soil-column model for the YY deposit (Figure 15a). This deposit is characterized by a shallow and relatively thick critical layer (zone), from 1.8 m to 6 m depth, with low penetration resistance of q_{c1Ncs} = 80 – 90. The critical layer is underlain by sand layers exhibiting higher and gradually increasing penetration resistance with depth. All top 10 m of the deposit are composed of liquefiable soils including the nominal crust above the water table.

Figure 16 shows computed time histories of excess pore water pressures throughout the depth of the deposit that reveal important liquefaction response features and interactions within the deposit. As indicated in Figure 16b and 16c, liquefaction was first triggered in the critical layer, at approximately t = 10 s on the computational time scale. The excess pore water pressures (u_E) build up rapidly and the critical layer quickly liquefies after only four seconds of strong shaking, approximately from t = 6 - 10 s. As illustrated in Figure 16d, the pore pressures also substantially increased in the denser sands beneath the critical layer, but these layers did not liquefy, as the excess pore water pressures did not reach the initial effective overburden stress (i.e. $u_E < \sigma'_{vo}$). However, the excess pore pressures in these deeper sand layers ($u_E \sim 70$ kPa) are substantially above the respective pressures in the critical layer, which range between 35 kPa and 65 kPa. This implies a significant inflow of water from the underlying deeper layers from 6 m to 10 m depth into the critical zone (layer), which will cause additional disturbance and instability through a prolonged and more severe fluidization of the already liquefied soils in the critical layer (zone). Finally, in Figure 16a a gradual increase in the excess pore water pressures is seen in the top part of the deposit, above the initial water table depth, due to upward flow of water from the liquefied critical layer towards the ground surface. These seepage-induced effects may further extend the liquefaction front towards the

ground surface, and eventually result in a liquefied deposit in the top 6 m with substantial inflow of water from deeper layers from 6 m to 10 depth. These mechanisms involving vertical communication of excess pore water pressures and large volumes of water create system response effects that intensify severity of liquefaction and associated damage (manifestation) at the ground surface.

Figure 17 schematically illustrates the principal mechanisms that lead to severe liquefaction manifestation at the ground surface of YY sites. They involve: (1) early and rapid liquefaction of the shallow critical layer; (2) additional disturbance of the liquefied critical layer due to substantial inflow of water from the underlying layers that didn't liquefy but generated high excess pore water pressures; and, (3) seepage-induced liquefaction in shallow soils above the water table. These system response effects result in a strong and damaging discharge of excess pore water pressures in which liquefiable soils from the entire deposit contribute to, and intensify, the severity of liquefaction manifestation. These insights from seismic effective stress analyses may explain the severe liquefaction manifestation observed at the YY-sites after the earthquakes.

4.5 *System response effects mitigating liquefaction manifestation*

The NN-deposit (Figure 15b) is also characterized by a shallow critical layer, from 2.5 m to 4 m depth, with equally low penetration resistance of q_{c1Ncs} = 80 as that of the YY-deposit. The key difference of this model is the presence of non-liquefiable layers and consequent vertical discontinuity of liquefiable layers. Another important feature of the NN-model is that a liquefiable layer of low penetration resistance is also encountered at larger depth, from 8.5 m to 10 m depth. Even though the water table is shallow at 1.6 m depth, there is a crust of non-liquefiable soil above the critical layer that prevents occurrence of seepage-induced liquefaction in near-surface soils. Hence, it is immediately obvious that mechanisms 2 and 3 intensifying liquefaction severity, identified for the YY-deposit (Figure 17), cannot develop in the NN-deposit.

Figure 18 shows maximum shear strains and horizontal accelerations computed throughout the NN-model. Liquefaction occurred in both the shallow critical layer (2.5-4.0 m depth) and the deep low resistance layer (8.5-10 m depth), with liquefaction triggering occurring only slightly faster in the deeper layer. The higher shear strains for the deeper layer reflect this nuance in the liquefaction response of the NN model. A significant effect of the liquefaction

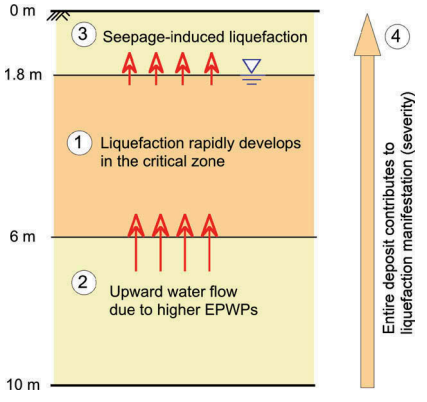

Figure 17. Schematic illustration of system-response mechanisms intensifying liquefaction manifestation (YY-sites) (Cubrinovski et al. 2018b).

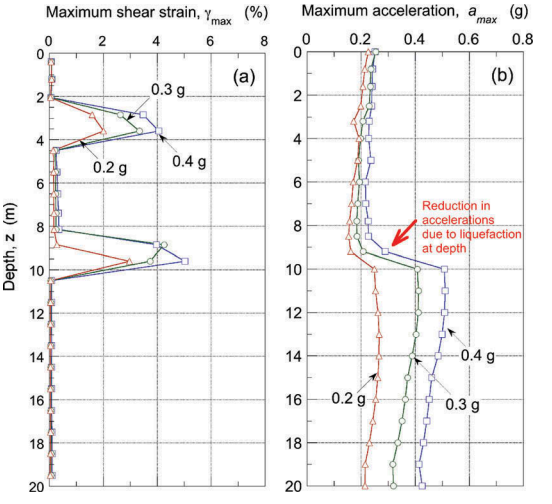

Figure 18. Computed response of the NN-model: (a) max. shear strains; (b) max. horizontal accelerations.

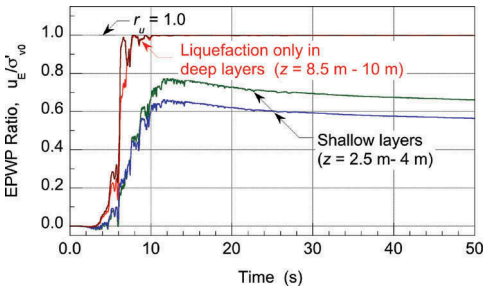

Figure 19. Excess pore water pressure time histories for shallow and deep liquefiable layers computed in analyses considering effects of partial saturation in shallow layers.

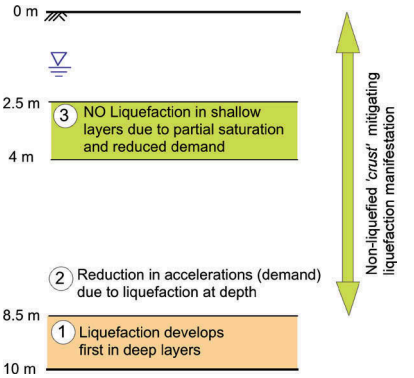

Figure 20. Schematic illustration of system response effects of liquefiable deposits that mitigate liquefaction manifestation (NN-sites).

in the deep layers is seen in Figure 18b, where sharp reduction in accelerations occurs from 10 m to 8.5 m depth due to liquefaction-induced softening of the deep loose layer. This 'base-isolation' effect has a profound influence on the overall deposit response, as it substantially reduces the inertial load for all soils above 8.5 m depth.

As mentioned previously, in the NN-deposits of interbedded liquefiable and non-liquefiable soils, partial saturation of soils was observed at depths within 3 m to 5 m below the water table, which implies that the shallow critical layer in the NN-deposit could be within the partially saturated zone. If an increased liquefaction resistance is assumed for the shallow critical layer due to partial saturation, then as illustrated in Figure 19, liquefaction will not occur in the shallow critical layer. Thus, combined effects of a reduced demand due to liquefaction in deep layers and an increased liquefaction resistance in shallow soils due to partial saturation may result in no liquefaction developing in the top 8.5 m of the deposit, and consequent absence of liquefaction manifestation at the ground surface.

Again, as in the case of the YY-deposit, cross-interactions between layers significantly modify the deposit response and influence liquefaction manifestation at the ground surface. However, unlike the mechanisms that intensify the severity of liquefaction for the YY-deposit, different mechanisms and interactions are at work for the NN-deposit, which mitigate development of liquefaction and its manifestation at the ground surface. Figure 20 illustrates key characteristics of the response and relevant mechanisms for the NN-sites. At these sites, liquefaction of the deep layer occurs first and produces the 'base-isolation' effect that substantially reduces the accelerations (and hence, the shear stresses) for all layers at shallower depths. This reduction in the seismic demand together with effects of partial saturation in the shallow parts of the highly-stratified deposit prevents occurrence of liquefaction in the shallow critical layer. As depicted schematically in Figure 20, this sequence of mitigating mechanisms effectively results in a non-liquefied 'crust' from the ground surface to 8.5 m depth, which prevents liquefaction manifestation at the ground surface, and is consistent with the absence of evidence of liquefaction at the ground surface of these sites after the Canterbury earthquakes.

The cascading mechanisms or system response effects work in opposite directions for the YY and NN sites with regard to liquefaction manifestation. For YY-sites, the system response effects increase the severity and consequences of liquefaction, whereas conversely, for the NN-sites, the interaction mechanisms mitigate liquefaction manifestation at the ground surface. In both cases, there are important cross-interactions between layers and different parts of the deposit through the dynamic response and water flow that substantially influence the development of liquefaction and even govern its manifestation at the ground surface. This clearly illustrates the need to incorporate system response effects in the assessment of liquefaction and associated damage.

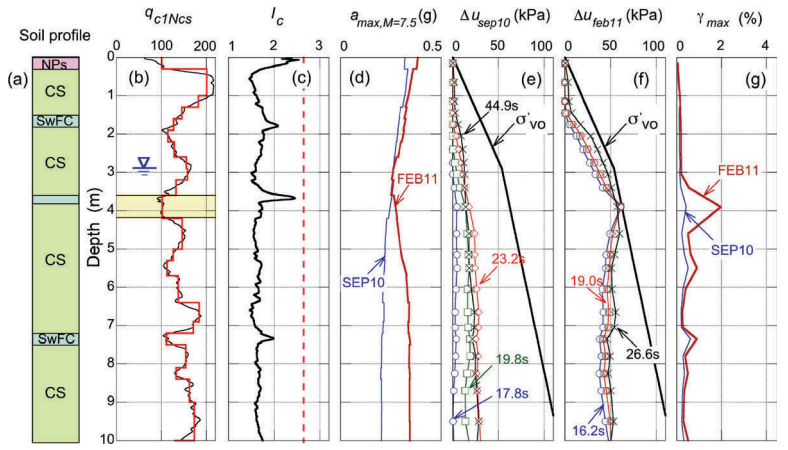

Figure 21. Characteristics of NY-1 deposit and computed response for SEP10 and FEB11 earthquakes: (a) simplified soil profile; (b) q_{c1Ncs} traces; (c) soil behavior type index, I_c; (d) maximum horizontal accelerations, $a_{max,M=7.5}$; (e-f) excess pore water pressures at different time sections; (g) maximum shear strains.

4.6 *Demand-dependent system response effects*

To further elucidate system response effects of liquefying deposits, results from seismic effective stress analyses are briefly discussed for two NY-sites, i.e. sites that did not manifest liquefaction in the 4 September 2010 (SEP10) event, but manifested liquefaction in the 22 February 2011 (FEB11) earthquake.

Simplified soil profile, CPT data and analyses results for the NY-1 site are shown in Figure 21. The NY-1 site has general deposit characteristics similar to those of the YY-sites, with vertically continuous liquefiable soils in the top 10 m of the deposit. However, the NY-1 site exhibits some subtle but important differences in details as compared to the YY soil profile (shown in Figure 15a). The critical layer of the NY-1 site is relatively thin and deeper (z_{CL} = 3.7 m), and it has slightly higher cone tip resistance of q_{c1Ncs} = 100. Also, the q_{c1Ncs} values are generally higher throughout the entire NY-1 profile.

Computed maximum accelerations, excess pore water pressures at different time sections during the strong shaking, and maximum shear strains are shown in Figures 21d to 21g, for the SEP10 and FEB11 earthquakes. Analysis results show that the demand imposed by the SEP10 earthquake was not sufficient to trigger liquefaction in the deposit, with excess pore water pressures remaining well below the initial effective vertical stress (Figure 21e), which is consistent with the absence of evidence of liquefaction at this site, after this event.

In contrast, for the FEB11 earthquake, analysis results indicate that liquefaction occurs in the critical layer at an early stage of the strong shaking (t = 16.2 s, Figure 21f). The computed excess pore water pressures in the deeper layers below the critical layer are at slightly lower level than those of the critical layer. This implies that mechanism 2 which is associated with strong inflow of water into the critical layer (depicted in Figure 17) could not develop in this case. Instead, these pressures will dissipate through a gradual and steady upward water flow towards the ground surface, which is evident in the gradual increase in the excess pore water pressures in the layers immediately above the critical layer. These system response effects are consistent with the moderate liquefaction manifestation observed at this site after the FEB11 earthquake.

Soil profile characteristics and results from effective stress analyses for the NY-2 site are shown in Figure 22. The NY-2 site has general characteristics similar to the NN deposits. It comprises interbedded liquefiable and non-liquefiable soils, with a thin non-liquefiable crust

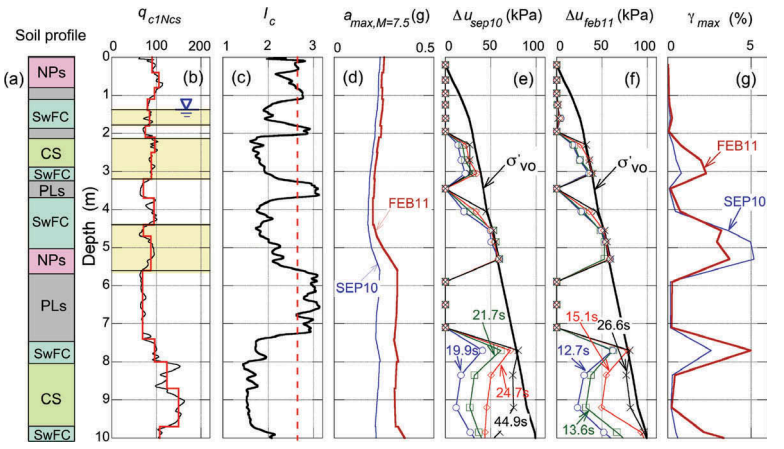

Figure 22. Characteristics of NY-2 deposit and computed response for SEP10 and FEB11 earthquakes: (a) simplified soil profile; (b) q_{c1Ncs} traces; (c) soil behavior type index, I_c; (d) maximum horizontal accelerations, $a_{max,M=7.5}$; (e-f) excess pore water pressures at different time sections; (g) maximum shear strains.

above the water table. It has a critical layer (zone) from 1.4 m to 3.0 m depth, but also liquefiable layers of low liquefaction resistance at greater depths, at 4.5 m and 7.5 m approximately.

Results from the seismic effective stress analyses for the SEP10 earthquake show that liquefaction developed in the layer from 4.4 m to 5.6 m depth at $t \approx 20$ s. At that time, the excess pore water pressures in the shallower layer at 2.1 m depth reached about 50% or less of the initial vertical effective stress, whereas no excess pore water pressures have developed in the shallowest critical layer. As illustrated in Figure 22d, the liquefaction at approximately 5 m depth caused a substantial reduction in the seismic demand for all soils above that depth, which prevented liquefaction developing in the shallow layers. This response features imply a non-liquefied crust from the ground surface to 4.4 m depth which could have prevented liquefaction manifestation at the ground surface for the relatively moderate amplitudes of shaking generated by this event.

A key difference in the response induced by the FEB11 earthquake simulation is that liquefaction also develops in the shallower layer from 2.1 m to 3.2 m depth due to the higher seismic demand imposed by this event. Consequently, in this case, the non-liquefied crust is only 2 m thick and could not prevent liquefaction manifestation under the severe amplitudes of shaking imposed by the FEB11 earthquake. Again, these results are in agreement with the moderate liquefaction manifestation observed at the NY-2 site after the 22 February 2011 earthquake.

A close scrutiny of the computed maximum shear strains shown in Figure 22g provides additional insights into the important differences between the response characteristics of the NY-2 deposit for the two events. A large concentration (i.e. localization) of shear strains is seen in the liquefied layer at approximately 5 m depth for the SEP10 earthquake, whereas the strains are substantially smaller in the shallower part of the deposit. Conversely, relatively large shear strains are seen throughout the entire deposit, at four different depths, in the FEB11 earthquake simulation. This implies that while in both cases liquefaction is predicted to occur, the overall response of the deposit would be significantly different for the two events with regard to liquefaction manifestation and associated damage in near-surface soils.

The liquefaction response features exemplified by the above NY-sites analyses, further emphasize the need to consider cross-layer interaction and system response effects in the assessment of liquefaction and its consequences. They illustrate that some of the mechanisms intensifying liquefaction manifestation, shown in Figure 17, may not develop if the demand is not sufficient to activate those mechanisms. Conversely, if the demand is very high, then some of the mechanisms mitigating liquefaction manifestation, shown in Figure 20, may not be

effective, as the relatively thin non-liquefiable layers and crust would be insufficient to prevent liquefied soils connecting vertically throughout the deposit, and eventually reaching the ground surface in the form of soil ejecta. These system response effects and demand-dependent mechanisms of interaction are currently the subject of a rigorous scrutiny through comprehensive series of seismic effective stress analyses.

5 CONCLUDING REMARKS

Soil liquefaction during earthquakes is a complex problem imposing numerous challenges in the engineering assessment. A large number of influencing factors are always in play that make a unique combination of contributions, and result in a particular set of response mechanisms, for given soil characteristics, ground conditions and earthquake excitation. Unweaving this complexity and identifying key factors and mechanisms that govern the liquefaction response and associated damage should be therefore one of the principal targets in the engineering assessment of liquefaction.

In order to evaluate effects of liquefaction and quantify damage to land and structures within performance-based design requirements, reasonably accurate estimates of transient and permanent ground displacements are needed for complex ground and soil-structure systems. The authors believe that these ambitious objectives in the assessment of liquefaction cannot be properly addressed without adequate consideration of material characterization, in-situ state characterization and system response effects of liquefiable deposits. Further advancements in this regard may bring a particular quality in the assessment through the ability to: 1) accurately discriminate between performances of different soils and ground conditions for a given earthquake excitation, and 2) accurately identify differences in performances of a given site for different earthquake excitations.

ACKNOWLEDGEMENTS

The first author would like to acknowledge the contributions of Claudio Cappellaro and Christopher de la Torre, PhD students at the University of Canterbury. Special thanks to our colleagues Prof. Brendon Bradley and Dr. Mark Stringer, University of Canterbury, Prof. Jonathan Bray, University of California, Berkeley, and Dr. Sjoerd van Ballegooy, Tonkin +Taylor, for their contributions to these research studies and comments on the draft of the paper. The Earthquake Commission New Zealand (EQC), QuakeCoRE, NZ Centre for Earthquake Resilience, MBIE and Natural Hazards Research Platform (NHRP) supported our research studies on the Canterbury and Kaikoura earthquakes.

REFERENCES

Beyzaei, C.Z., Bray, J.D., van Ballegooy, S., Cubrinovski, M., Bastin, S. 2018. Depositional Environment Effects on Observed Liquefaction Performance in Silt Swamps during the Canterbury Earthquake Sequence. *Soil Dynamics and Earthquake Engineering*, 107: 303–321.

Boulanger, R.W. & Idriss, I.M. 2014. *CPT and SPT Based Liquefaction Triggering Procedures*. Report No. UCD/CGM-14/01, Center for Geotechnical Modeling, University of California, Davis, April 2014.

Bradley, B., Razafindrakoto, H.N.T., & Polak, V. 2017. Ground motion observations from the 14 November 2016 Mw7.8 Kaikoura, New Zealand earthquake and insights from broadband simulations, *Seismological Research Letters*, 88(3): 740–756.

Bray, J., Cubrinovski, M., Zupan, J., & Taylor, M. 2014. Liquefaction effects on buildings in the central business district of Christchurch. *Earthquake Spectra*, *30*(1), 85–109. doi:10.1193/022113EQS043M

Cubrinovski, M., & Ishihara, K. 1999. Empirical correlation between SPT N-value and relative density for sandy soils. *Soils and Foundations*, *39*(5): 61–71.

Cubrinovski, M., & Ishihara, K. 2000. Flow potential of sandy soils with different grain compositions. *Soils and Foundations*, *40*(4): 103–119.

Cubrinovski, M., & Ishihara, K. 2002. Maximum and minimum void ratio characteristics of sands. *Soils and Foundations*, *42*(6): 65–78.

Cubrinovski, M., Bradley, B., Wotherspoon, L., Green, R., Bray, J., Wood, C., … Wells, D. 2011a. Geotechnical aspects of the 22 February 2011 Christchurch earthquake. *Bulletin of the New Zealand Society for Earthquake Engineering*, *44*(4): 205–226.

Cubrinovski, M., Winkley, A., Haskell, J., Palermo, A., Wotherspoon, L., Robinson, K., … Hughes, M. 2014a. Spreading-induced damage to short-span bridges in Christchurch, New Zealand. *Earthquake Spectra*, *30*(1), 57–83. doi:10.1193/030513EQS063M

Cubrinovski, M., Hughes, M., & O'Rourke, T. D. 2014b. Impacts of liquefaction on the potable water system of Christchurch in the 2010-2011 Canterbury (NZ) earthquakes. *Journal of Water Supply: Research and Technology - AQUA*, *63*(2), 95–105. doi:10.2166/aqua.2013.004

Cubrinovski, M., Bray, J., de la Torre, C., Olsen, M., Bradley, B., Chiaro, G., Stocks, E., Wotherspoon, L. & Krall, T. 2017. Liquefaction effects and associated damages observed at the Wellington CentrePort from the 2016 Kaikoura earthquake. *Bulletin of the New Zealand Society for Earthquake Engineering*, 50(2): 152–173.

Cubrinovski, M., Bray, J., de la Torre, C., Olsen, M., Bradley, B., Chiaro, G., Stocks, E. & Wotherspoon, L. 2018a. Liquefaction–induced damage and CPT characterization of the reclamations at CentrePort, Wellington. *Bulletin of the Seismological Society of America*, 108(3B): 1695–1708.

Cubrinovski, M., Rhodes, A., Ntritsos, N. & van Ballegooy, S. 2018b. System response of liquefiable deposits. *Soil Dynamics and Earthquake Engineering*, available online, 10.1016/j.soildyn.2018.05.013

Dhakal, R., Cubrinovski, M., de la Torre, C. & Bray, J. 2019. Site characterization for liquefaction assessment of gravelly reclamations at CentrePort, Wellington, *Proc. 7ICEGE*, 17-20 June 2019, Rome, Italy.

Idriss I.M. & Boulanger R.W. 2008. *Soil liquefaction during earthquakes*. Monograph MNO-12. Oakland, CA: Earthquake Engineering Research Institute; 261.

Iwasaki, T., Tatsuoka, F., Tokida, K., & Yasuda, S. 1978. "A practical method for assessing soil liquefaction potential based on case studies at various sites in Japan." *Proc., 2nd Int. Conf. on Microzonation*, Washington, DC.

Lade, P.V., Liggio, C.D. & Yamamuro J.A. 1998. Effects of non-plastic fnes on minimum and maximum void ratios of sand, *Geotechnical Testing Journal*, GTJODJ, 21(4):336–347.

Maurer, B., Green, R., Cubrinovski, M., & Bradley, B. 2014. Evaluation of the Liquefaction Potential Index for Assessing Liquefaction Hazard in Christchurch, New Zealand. *Journal of Geotechnical and Geoenvironmental Eng*., ASCE, 140(7).10.1061/(ASCE)GT.1943-5606.0001117

Robertson P.K., Campanella, R.G. & Wightman A. 1983. SPT–CPT correlations. *J. of Geotechnical Engineering*, ASCE, 109(11): 1449–1459.

Robertson P.K. & Wride C.E. 1998. Evaluating cyclic liquefaction potential using cone penetration test. *CanGeotechJ* 35(3): 442–459.

Robertson P.K. 2012. Interpretation of in-situ tests – some insights, Mitchell Lecture, ISC'4, Brazil, September 2012, 1–22.

Robertson P.K. & Cabal K.I. 2012. Cone Penetration Testing for Geotechnical Engineering, Gregg Drilling & Testing, Inc., p.131.

Skempton, A. W. 1986. Standard penetration test procedures and the effects ins ands of overburden stress, relative density, particle size, aging and overconsolidation. *Geotechnique*, 36(3): 425–447.

Tatsuoka, F., Zhou, S., Sato, T., & Shibuya, S. 1990. Method of evaluating liquefaction potential and its application. Rep. on Seismic hazards in the soil deposits in urban areas, Ministry of Education of Japan, 75–109 (in Japanese).

Tokimatsu, K. 1988. Penetration tests for dynamic problems, *Proc. Penetration Testing ISOPT-1*, 117–136.

Van Ballegooy, S., Malan, P., Lacrosse, V., Jacka, M. E., Cubrinovski, M., Bray, J. D., … Cowan, H. 2014. Assessment of liquefaction-induced land damage for residential Christchurch. *Earthquake Spectra*, *30*(1), 31–55. doi:10.1193/031813EQS070M

Youd, T.L., Idriss, I.M., Andrus, R.D., Arango, I., Castro, G., … 2001. Liquefaction resistance of soils: summary report from the 1996 NCEER and 1998 NCEER/NSF workshops on evaluation of liquefaction resistance of soils, *J. Geotechnical and Geoenvironmental Eng*., ASCE 127(10): 817–833.

Zhang, G., Robertson, P. K., & Brachman, R. W. I. 2004. Estimating Liquefaction-Induced Lateral Displacements Using the Standard Penetration Test or Cone Penetration Test. *Journal of Geotechnical and Geoenvironmental Engineering*, ASCE, 130(8): 861–871.